Interplay between structural, chemical, and spectroscopic properties of Ag/Au(111) epitaxial ultrathin films: A way to tune the Rashba coupling

H. Cercellier, C. Didiot, Y. Fagot-Revurat, B. Kierren, L. Moreau, and D. Malterre
Laboratoire de Physique des Matériaux, Université Henri Poincaré, Nancy I - B.P. 239 F-54506 Vandœuvre-lès-Nancy, France

F. Reinert
Experimentelle Physik II, Universität Würzburg, Am Hubland, D-97074 Würzburg, Germany
(Received 17 October 2005; revised manuscript received 10 March 2006; published 16 May 2006)

An overview of structural, chemical, and electronic properties of epitaxial Ag/Au(111) ultrathin films investigated by scanning tunneling microscopy and scanning tunneling spectroscopy and angle-resolved photoelectron spectroscopy is presented. New insights are exhibited: (i) a short-range ordered surface reconstruction is clearly observed for deposition at 300 K; (ii) self-organized ordering of Ag islands is obtained at $T \simeq 80$ K. In this whole temperature range, the Ag/Au(111) interface is shown to be (nearly) abrupt. An annealing of the elaborated room temperature leads to a strong intermixing and favors the formation of a chemically disordered surface alloy. The Shockley state parameters have been fully characterized for both interfaces. Surprisingly, the Rashba parameter is shown to scale the binding energy of the surface state in both cases. A simple one-dimensional model, taking into account the exponential decrease of the surface state wave function, allows us a quantitative understanding of the evolution of the surface state parameters. Indeed, the strength of the spin-orbit splitting is shown to be proportional to the number of heavy atoms probed by the surface state wave function, revealing its atomic character. Therefore, the strength of the Rasba coupling is shown to be tuned by adjusting the number of Ag epitaxial layers or the Ag-Au alloy composition.

DOI: 10.1103/PhysRevB.73.195413 PACS number(s): 73.20.At, 79.60.−i, 68.37.Ef, 71.70.Ej

I. INTRODUCTION

Surface physics has been termed as one of the "playgrounds" of physics: (i) The change of thermodynamical conditions in the vicinity of the surface allows us to create unusual phases and/or interfaces (surface reconstructions, unusual crystallographic structure, etc.) inducing singular electronic properties; (ii) the breakdown of the translational invariance in the direction normal to the surface leads to the appearance of different surface and interface electronic states which play a fundamental role in surface science.[1–4] Indeed, these states can be used as spectroscopic probe of surface and interface phenomena,[5,6] they can influence the growth,[7] drive the self-organization of adatoms at low temperature,[8] and can also be used to control the surface reactivity.[9] These surface state electrons, especially *L*-gap Shockley states appearing on noble metal surface, can also be used in a very simple way for testing very fundamental physical concepts, even beyond surface science. They obey in a first approximation the simplest physical model which can be drawn for electrons in solids, i.e., the nearly free electronlike model (NFE) with parabolic energy dispersion curves. Their localization at the surface makes them strongly sensitive to any surface perturbation. Their binding energy can be modified by changing the work function (alkali adsorption),[5] the dielectric constant outside the barrier (rare gas adsorption[10] and insulating barriers[11]), or the amplitude of the surface electronic potential (in the case of metal-metal growth of ultrathin film, reconstructions,…).[6] Confinement in nanoscale objects (between steps on vicinal surfaces or in islands) are also known to modify the intrinsic surface state energies.[12] The Au(111) surface band is known to be unique since it presents a *k*-dependent spin-orbit splitting due to the breakdown of the inversion symmetry at the surface.[13] As a consequence, the surface electrons carry magnetic information and this opens a new field of investigation such as scattering of surface states by magnetic objects. This could be relevant since spin-polarized surface and interface states are known to play a fundamental role in spintronics.[14] The spin-orbit Hamiltonian is usually expressed by

$$H_{SO} = \frac{\hbar}{4m^2c^2}(\vec{\nabla}V \times \vec{p}) \cdot \vec{\sigma}, \tag{1}$$

where V is the potential, $\vec{p}$ the electron momentum, and $\vec{\sigma}$ the spin quantum number. In the case of atomic levels, it can be written as proportional to $\vec{L}\vec{S}$, where $\vec{L}$ and $\vec{S}$ are the angular and spin momentum, respectively. Therefore, the degeneracy is partially resolved by adding this relativistic correction, its strength increasing with the atomic number Z and the electron velocity. This effect, well-known in atomic physics, exists also in solids leading to an energy splitting as observed in the band structure of semiconductors.[15] Moreover, an additional spin-orbit *k*-splitting should be observable in band states depending on the crystal symmetry: for centrosymmetric crystals like in Ge, the inversion center coupled with the time-reversal symmetry leads to a degeneracy as a function of the momentum projection $E(\vec{k},\sigma^+)=E(\vec{k},\sigma^-)$; on the contrary, for noncentrosymmetric crystals like zinc blende crystal structure (CdTe), this degeneracy is resolved so that $E(\vec{k},\sigma^+) \neq E(\vec{k},\sigma^-)$, leading to the occurrence of spin-polarized subbands as discussed a long time ago for band structure of semiconductors.[16–18] Therefore, no sign of such a *k*-splitting should be observable on the band structure of

noble metals having a fcc crystal structure. Nevertheless, the surface breaks the inversion symmetry in the normal direction, revealing a substantial splitting on the Au(111) Shockley state.[13] Later on, such splitting was reported for surface states observed on W(110) and Mo(110) surfaces.[19,20] The consequence of the spin-orbit interaction on a two-dimensional gas of nearly free electrons (known as the Rashba effect) was formalized in 1960 to describe the spin-splitting observed in asymmetric quantum wells.[21] Assuming the NFE nature of the 2D Shockley states considered here and their localization in the vicinity of the surface where the potential gradient normal to the surface is large enough, the Rashba theory was first applied to these states.[13] The potential gradient in the direction normal to the surface plane is written as $\vec{\nabla} V = \frac{dV}{dz}\vec{e_z}$. The electron momentum $\vec{p}_{//} = \hbar \vec{k}_{//}$ lies in the surface plane and the following Rashba Hamiltonian is derived:

$$H_R = \alpha_R (\vec{e_z} \times \vec{k}_{//}) \cdot \vec{\sigma}. \tag{2}$$

α_R defines the Rashba parameter proportional to the potential gradient felt by the surface electrons. The effect of the Rashba Hamiltonian is to lift the spin degeneracy by adding to the NFE parabolic dispersion an additional term proportional to $k_{//}$ leading to the new spin-dependent dispersion relations,

$$E_{\pm}(k_{//}, \sigma^{\pm}) = \hbar^2 k_{//}^2 / 2m^* \pm \alpha_R k_{//} \tag{3}$$

(± defining here the two opposite directions of spin-polarization). Such dispersion curves give rise to a split Fermi surface as demonstrated by high-resolution angle-resolved photoelectron spectroscopy (ARPES) experiments recently performed.[22] Later on, the magnetic origin of such splitting was established with the development of spin-resolved photoemission spectroscopy (SR-ARPES) first in the case of $W(110)-(1\times 1)H$ surface states[23] and then for the Au(111) Shockley state.[24] These states have been shown to be 100% spin-polarized as expected theoretically.[25] As mentioned in the initial work of LaShell *et al.*,[13] in the jellium model, the surface potential varies on the order of the work function on a length scale of the order of the Fermi wavelength, giving a negligible splitting $\approx 10^{-6}$ eV compared to the one measured for Au(111) ($\approx$0.11 eV). It has been shown that a more realistic model which takes into account the core potential component of the potential gradient restores a splitting proportional to the atomic spin-orbit coupling.[13,26] Then, this effect should be stronger for heavy atoms and explain why no sign of spin-splitting has been evidenced on the Ag(111) *L*-gap surface state up to now. *Ab initio* calculations give the correct value for Au(111) surface state and predict a very small splitting on Ag(111), of the order of the experimental resolution available in recent photoemission setup.[27] Adsorption of Xe on Au(111) (Ref. 27) and Li on W(110) (Ref. 20) leads to an increase in this spin-orbit splitting, but the explanations for that remain unclear. Therefore, since the strength of the coupling should depend on the work function and/or the presence of heavy atoms in the vicinity of the surface, it is of great interest to measure quantitatively the Au(111) surface state properties modified by Ag epitaxial ultrathin films. Nevertheless, the structure and the morphology of the Ag/Au(111) interface should be well controlled.[28,29] Some experimental works have been published already on the growth of Ag on Au(111).[30–32] We have already published a comparison between some of the ARPES data presented here and band-structure calculations.[33] Nevertheless, to the best of our knowledge, a comprehensive understanding of surface state properties correlated with the growth of Ag thin films on Au(111) has not been published up to now. This is the purpose of this paper.

Ag and Au noble metals have a face-centered cubic structure. The Au(111) surface presents a herringbonelike surface reconstruction, consisting of the alternation of hexagonal compact (hcp) and face-centered cubic (fcc) areas separated by stacking fault lines with a superperiodicity of 63 Å.[34–36] Such surface reconstruction has not been evidenced for the Ag(111) bare surface. Moreover, reconstructed Ag islands have been observed for ultrathin Ag films [for two layers of Ag deposited on Pt(111) (Ref. 37) and for Ag films deposited on Ru(0001) (Ref. 38)], and the degeneracy of hcp and fcc domains seems to be a common feature of hexagonal surface. Usually, a strong misfit parameter leads to reconstructed thin films as observed for Au/Ni(111) (Ref. 39) or Ag/Cu(111) (Refs. 40 and 41). The large lattice mismatch in the latter system is responsible for the observed superstructure at surface. Despite the negligible misfit parameters (0.2%) between Au(111) and Ag(111) surfaces, the pre-existing substrate reconstruction should influence the Ag epitaxial growth, at least in the early stage of growth as has been shown, e.g., for transition metal thin films.[42,43] In addition, Ag and Au atoms are known to be miscible in the bulk. This property has been used to form a surface alloy whereas deposition at low temperature ($\leqslant$300 K) leads to an abrupt Ag/Au(111) interface.

In this paper, the singular growth of Ag films deposited on Au(111) is addressed in detail and reviewed: the first, second, and third Ag layers obtained for room-temperature deposition are shown to be reconstructed—self-organization of Ag islands at low T is clearly established—a disordered surface alloy with tunable Ag-Au composition is obtained by annealing Ag thin films above the room temperature. Thus, the perfect control of the Ag/Au(111) interface (morphology and chemical composition) allows us to understand quantitatively the evolution of the Shockley state parameters. In particular, we focus on the binding energy and the spin-orbit splitting. The experimental work presented here evidences that the Rashba effect observed on Shockley states depends only on the relative amount of Au (heavy atoms) and Ag atoms probed by the surface state wave function: (i) in the case of the abrupt Ag/Au(111) interface, the number of Au atoms probed by the surface state wave function is decreased by increasing the Ag layer thickness; (ii) in the alloy, however, it is increased by enriching the surface in Au atoms by adjusting the annealing temperature. In both cases, the spin-orbit splitting scales the binding energy and does not scale the work function of the Ag film. A simple one-dimensional model based on a pseudopotential formalism is used to explain the experimental measurements presented here quantitatively.

This paper is organized as follows: Experimental details concerning scanning tunneling microscopy (STM), scanning tunneling spectroscopy (STS), ARPES, AES (Auger-electron spectroscopy), and work function measurements are presented in Section II. Section III is devoted to the experimental results. STM and AES measurements are first used to discuss the structure, the morphology, and the chemical composition of the Ag/Au(111) interface as function of the Ag coverage and of the temperature (Sec. III A). Then, the Shockley state parameters are extracted from ARPES and STS data in the case of the abrupt interface and for the Ag -Au alloy (Sec. III B). For both cases, the Rashba parameter is shown to scale the binding energy of the surface state. Calculations based on a one-dimensional pseudopotential formalism are presented in Sec. IV. A simple one-dimensional diffusion model is used to describe the surface alloy formation (Sec. IV C). Our simple calculations are shown to capture the essence of the experimental variation observed in the Shockley state parameters. A summary is presented in Sec. V.

II. EXPERIMENTAL DETAILS

The measurements were carried out in an UHV setup composed of a molecular beam epitaxy chamber for the elaboration and characterization of the surfaces, a STM chamber equipped with an Omicron LT-STM operating in the temperature range 17–300 K, and a photoemission chamber with a high-resolution Scienta SES 200 analyzer. The photoemission experiments can be recorded between 20 K and room temperature. The He-I ($h\nu$=21.2 eV), and Ar-I ($h\nu$ =11.82 and 11.62 eV) radiations are provided by a high-intensity UVS-300 SPECS discharge lamp operating at a pressure of 10^{-5} mbar in the ionization chamber. The energy resolution of the ARPES analyzer was better than 5 meV and angular resolution better than 0.4 deg, corresponding to a k resolution better than 0.015 $Å^{-1}$ in He-I mode and 0.010 $Å^{-1}$ in Ar-I mode. The electrons are collected by a microchannel plate and accelerated onto a phosphorus screen monitored by a charge-coupled device (CCD) camera. This 2D detector allows us to record accurately the emission spectra between −6 and +6 deg in less than 10 min and permits us to avoid surface contaminations. All the ARPES spectra presented here have been measured at a fixed temperature of 90 K in pressure of 10^{-9} mbar during UV excitation, the base pressure being less than 10^{-10} mbar. The STS spectra have been obtained at 60 K (solid nitrogen temperature) by measuring the differential conductivity recorded with a locking technique. A voltage modulation of 7–14 mV (rms) is added to the junction bias with a frequency of 650 Hz with a time constant lower than 10 ms. We used cut Pt-Ir and tungsten electrochemically etched tips. Both were sputtered with Ar ions and annealed *in situ*. The commercial Au(111) substrate was first prepared by a mechanical polishing and aligned in the (111) direction with an accuracy better than 0.1 deg. After introduction in the UHV setup, the substrate was cleaned by several cycles of Ar^+ etching at 2 keV and annealing at 650–900 K. The quality, cleanliness and morphology of the sample were characterized by Auger electron spectroscopy (AES) and by checking the herringbone reconstruction by STM. The Ag atoms were evaporated from a Knudsen cell operating at T=1320 K at a rate in the range of 0.5–2 ML/mn. This rate was measured by monitoring the frequency shift of a quartz microbalance with a 12-digit counter. The calibration was checked by STM measurements corroborated by AES data. During Ag deposition, the substrate temperature could be adjusted in the range 80–300 K. An annealing up to 600 K has been used to create the Ag -Au alloy. The work function ϕ_S has been measured by AES and ARPES: the relative variation of ϕ_S as function of the deposition or annealing has been obtained by measuring the secondary electron's step edge with the AES analyzer, the sample being polarized at 50 V. The absolute value of ϕ_S for Au(111) was provided by the secondary electron edge given by the difference between the sample work function ϕ_S and the analyzer work function ϕ_{ANA} which is well known from ARPES measurements. The experimental values obtained for Au(111)(ϕ_S=5.34 eV) and thick Ag layers (ϕ_S=4.29 eV) are in good agreement with the published data.[45]

III. RESULTS AND DISCUSSION

A. Structure and morphology of the Ag/Au(111) interface

1. Ag films elaborated at 300 K

STM images of room-temperature, deposition of Ag on a Au(111) substrate are presented for different coverages in Fig. 1. As already observed for the Ag/Cu(111) epitaxial interface,[46] the Ag islands are of monoatomic height and connected to step edges [Fig. 1]. The diffusion length of Ag adatoms is probably more than several hundred angstroms so that step edges are nucleation centers. At this temperature, very distorted islands are observed due to the high mobility of Ag adatoms. The growth of the second layer starts after completion of the first one as shown in Fig. 1(b). According to the literature,[30,31] a nearly layer-by-layer growth is observed at room temperature at least up to 5 ML (only monoatomic terraces are seen for a coverage of 4.5 monolayers of Ag). However, STS (not presented here) has revealed a subtle deviation to a pure layer-by-layer growth as described in a recent paper.[47] In Fig. 1(c), we can identify the typical $22\times\sqrt{3}$ herringbone surface reconstruction of the Au(111) substrate:[34–36] an alternation of hcp and fcc domains separated by stacking fault lines along the $[10\bar{1}]$ direction responsible for the small corrugations (0.2 Å) observed in STM. The uniaxial compression in this direction allows a ratio of 23 surface Au atoms for 22 in the bulk leading to a superperiodicity of 63 Å.[48,49] The threefold symmetry of the (111) surface leads to three 120 deg turned distinct domains separated by dislocation loops aligned along the $[1\bar{2}1]$ direction. We would like to point out additional insights.[30,31] The Ag islands of monoatomic height [Fig. 1(a) show small corrugations (≈0.2 Å) defining alternating dark and bright domains. The superperiodicity observed in Ag islands is the same as the one of the underlying Au(111) surface reconstruction as evidenced by the z-profiles presented in Fig. 1(e). The typical sizes for dark and bright domains evaluated in Figs. 1(c) and

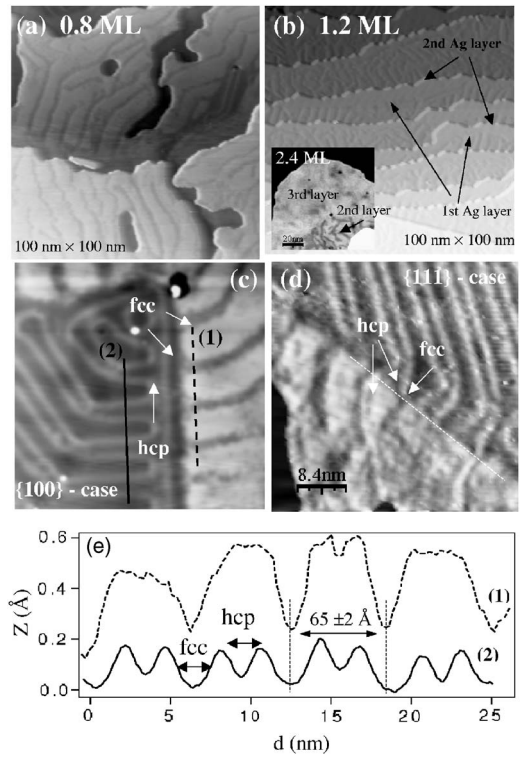

FIG. 1. Topographic STM images of (a) 0.8 and (b) 1.2 Ag layers deposited on Au(111) at 300 K; inset: 2.4 Ag monolayer deposition evidencing the reconstructed second and third Ag layers;(c) reconstructed first Ag layer close to a {100} step; (d) close to a {111} step; (e) *z*-profile evidencing the superperiodicity observed both on Au(111) substrate and monoatomic Ag islands.

1(d) are approximately 25 and 35 Å, comparable to the typical size of hcp and fcc domains of the Au(111) substrate, respectively. Nevertheless, note that the large domains correspond to Ag growth on hcp domains including stacking fault lines, whereas small domains correspond to a growth on reduced fcc domains. As already discussed in the literature for Au(111) surface,[50] we observed that discommensuration lines behave differently depending on the type of close-packed steps encountered. In the case of a {100} microfacet, the discommensuration lines coming at the top of the step avoid crossing the steps, leading to a stacking fault line parallel to the step edges. In this case, Au atoms located at the step edge are in regular fcc stacking.[50] In addition, at the bottom of the step edges the discommensuration lines are perpendicular to the step edge with an alternation of hcp and fcc stacking for atoms close to the step edge. In the case of {111} microfacets, the fault lines go through the {111} step edges on both sides of the step. Here, Ag islands have the tendency to build local {111} microfacets in order to minimize the interaction energy between reconstruction and steps (not presented here).

If we consider now the Ag islands connected to {100} [Fig. 1(c)] or {111} [Fig. 1(d)] microfacets, we can also draw some conclusions. Taking into account the fact that Au atoms closer to the {100} step edges are in fcc stacking, it appears that the dark domains inside the Ag islands correspond also to a fcc stacking. Indeed, it appears at the same height and no

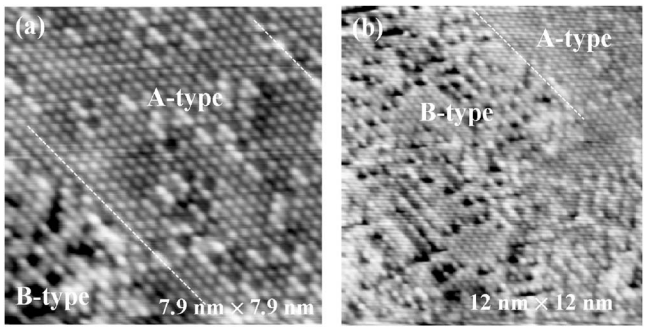

FIG. 2. Atomically resolved STM image obtained mainly on the bright (a) and dark (b) domains.

discommensuration lines cross the domains. Moreover, in the case of Ag islands connected to {111} microfacets, it appears clearly that the fault lines arriving perpendicular to the steps cross the step edge into the Ag islands, the bright domains observed in Ag islands being directly connected to the hcp stacking. The size of the bright domains observed in Ag islands corresponds to the size of hcp domains including the fault lines [see the *z*-profile in Fig. 1(e)]. In addition, smaller but non-negligible corrugations are evidenced in the second and third Ag layer [inset, Fig. 1(b)] with a strong disordered character. A careful STS investigation of the surface state behavior shows different spectroscopic signature for the dark and bright domains as presented in Sec. III B 2. Therefore, for Ag deposition at 300 K, a well- characterized short-range ordered reconstruction is evidenced in the first Ag layer. Reminiscent features of this reconstruction are also evidenced in the second and third layers. Atomic resolution inside the domains observed on the first layer is shown in Figs. 2(a) and 2(b). Despite the good crystallographic alignment, some contrast appears inside the Ag domains at atomic scale. Few atoms of the Ag layer appear darker, whereas the six surrounding atoms are brighter. This has been observed already in other metal/metal interface.[39] It is usually assumed to be chemical contrast due to the inclusion of different chemical species in the layer which could be Au atoms in this case. The STM image presented in Fig. 2(b) has been taken by moving the tip from an area with mainly a bright domain (*A* type) through an area with mainly dark domains (*B* type). The number of inclusions is clearly larger for dark domains than for bright ones. This indicates a preferential segregation of Au atoms coming from fcc domains. Unfortunately, we do not have enough STM images with such high resolution to quantify the number of inclusions but we estimate it is less than 8%. This small interdiffusion at room temperature is supported by optical measurements evidencing segregation of a few percent of Au atoms in the Ag/Au(111) interface, whereas no intermixing is observed on the Ag/Cu(111) system.[51] As discussed in Sec. III A 3, an annealing increases this intermixing and yields to the formation of a Ag-Au surface alloy.

Starting from these experimental evidences, we try to propose a scenario to explain the reconstructed Ag islands. The Au(111) surface plane relaxes the surface elastic strains through the $22\times\sqrt{3}$ reconstruction. The mismatch between Ag and Au lattices is very weak (0.2%). The two materials

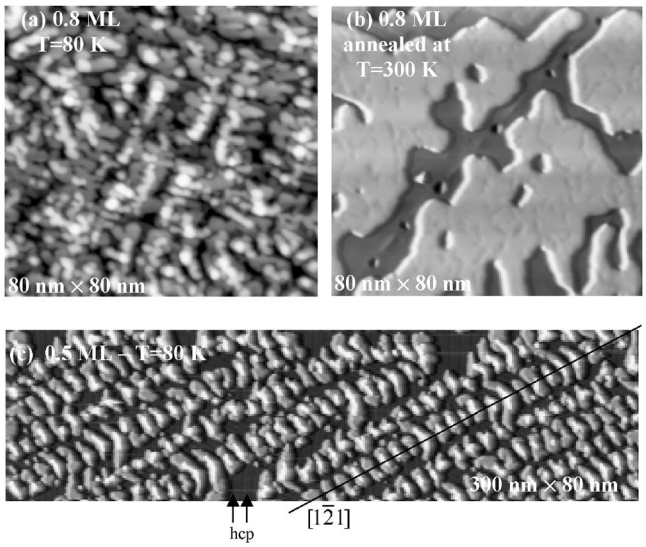

FIG. 3. (a) STM image of 0.8 Ag ML deposited on Au(111) at 80 K; (b) 0.8 ML after thermalization at 300 K; (c) case of 0.5 ML evidencing self-organization of Ag islands at 80 K.

are fully miscible in the bulk, leading to chemically disordered $Au_{1-x}Ag_x$ solid solutions. In addition, the Au atom surface energy (γ_s=2.66 J m^{-2}) is larger than the Ag one (γ_s=1.20 J m^{-2}), which should not favor intermixing. Nevertheless, as soon as the last Au(111) plane is covered by Ag adatoms, it becomes a subsurface plane. Therefore, it could be energetically unfavorable to keep 23 Au atoms (instead of 22) inside this plane and the 5% of additional Au atoms may diffuse in the Ag layer. This can explain qualitatively the chemical contrast observed at atomic scale. Therefore, this contrast observed between bright and dark areas could be related to the different number of Au inclusions as suggested by the results presented in Fig. 2. Then, the diffusion of Au atoms should be different for Au atoms coming from hcp or fcc domains of the subsurface plane and could be the driving force of the superstructure observed in the Ag layer. To our knowledge, such preferential interdiffusion between the two kinds of domains has not been observed in other metal-metal systems. Moreover, we cannot exclude that Au(111) reconstruction could be preserved in the covered Au plane, the small corrugations observed on the Ag islands revealing the persistent subsurface reconstruction. Further experimental investigations including subsurface sensitive techniques would be of great interest in order to go beyond this STM investigation.

2. Self-organized Ag growth at 80 K

A different morphology can be obtained by changing the temperature of the substrate. The case of low-T deposition of Ag on Au(111) is discussed here. Deposition of 0.8 ML Ag on Au(111) substrate cooled at 80 K is presented in Fig. 3. At this temperature, three-dimensional Ag islands are clearly observed. By increasing the substrate temperature from 80 to 300 K the Ag layer is smoothed and small disordered corrugations are created. A slow decrease of the AES Au line intensity observed with increasing the substrate temperature corroborates this transition from 3D islands to 2D films [see Fig. 4(a)]. The long-range order observed on Ag reconstructed islands for films prepared at room temperature is not recovered. Depositions at room temperature or at low T fol-

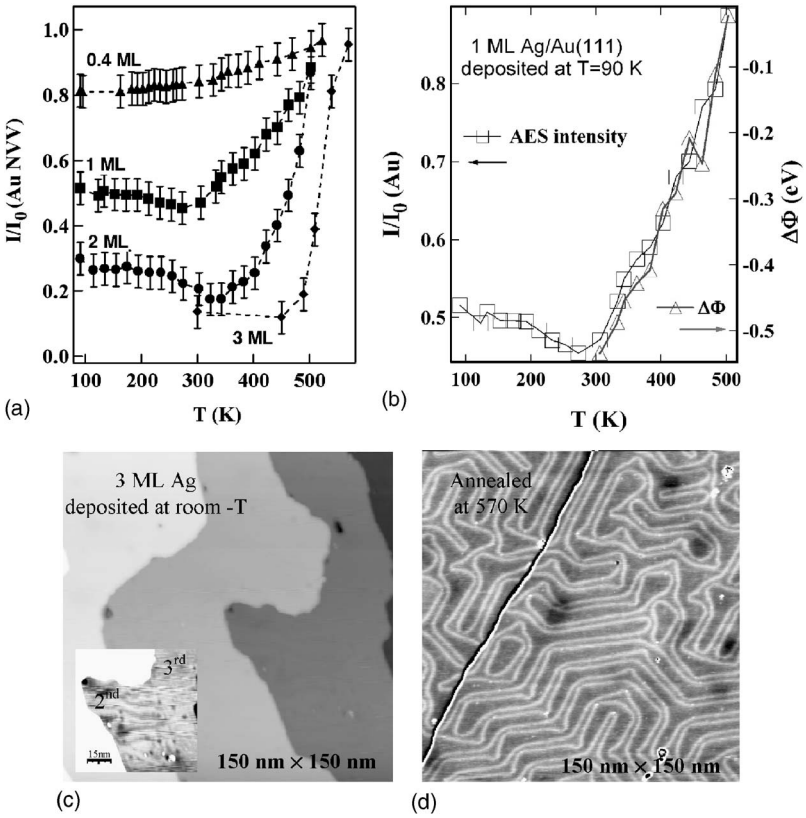

FIG. 4. (a) AES low-energy (NVV) Au line intensity (I) normalized to the intensity on free Au(111) surface (I_0); (b) work function modification measured as function of the annealing temperature for one Ag monolayer coverage— $\Delta\Phi$ is referred to the bare Au(111) surface value; (c) STM image obtained for 3 Ag monolayers deposited at room temperature; (d) same film after annealing at 570 K.

lowed by an annealing lead to different ordering of the reconstructed layer. A STM image of a 0.5 ML film deposited at 80 K is presented in Fig. 3(b), shedding some light on the possibility for self-organization at low T. Ag islands obtained at 80 K have a singular crescent shape for very low coverage. The herringbone Au(111) reconstruction is well known to strongly influence epitaxial growth: the dislocation loops introduce some preferential adsorption sites at the elbows of the reconstruction, which are pinning centers for various adsorbed chemical species like Ni,[42] Co,[43] and Fe atoms.[44] This property has been intensively used to create nanodotted surfaces, especially on vicinal surfaces.[52] For the growth of Ag on Au(111) at low T, Ag islands are strongly anisotropic and evidence a preferential nucleation of Ag atoms mostly on hcp domains of the substrate reconstruction, including the stacking fault lines. This is in agreement with a previous STM study.[30] This is in clear contradiction to the growth mode observed for Co (and Ni), where the elbow of the herringbone reconstruction is shown to be the unique preferential growth site. Indeed, a two-step process including first an exchange between adsorbate species and Au substrate atoms was evidenced for the first stage of growth.[53] Then, due to a strong Co-Co interaction, isotropic Co bilayer islands can grow. In the case of Ag/Au(111), the activation energy responsible for trapping Ag adatoms is lower than for Co since a relatively low temperature is needed for self-organization of Ag islands. In addition, if the elbow site seems to be a preferential site, Ag islands grow on the entire hcp domain as revealed by Fig. 3(c). Since each vertex of the substrate reconstruction is occupied by a Ag island, a long-range ordering is obtained along the $[1\bar{2}1]$ direction. In the case of small terraces, Ag adatoms present a regular pattern which would allow us to create a regular array of Ag islands on vicinal surfaces favoring very well-ordered nanostructures.[54] A more detailed study of the shape of the islands as function of the size of the terraces, especially on vicinal surfaces, will be presented in a forthcoming paper.

3. *Films annealed above* 300 K*: Alloy formation*

We investigated annealed Ag layers by AES spectroscopy, work function measurements, and STM. The results are presented in Fig. 4. The low-energy (69 eV) Au NVV AES transition has been monitored as function of temperature for several coverages [Fig. 4(a)]. Two distinct regimes can be evidenced. First, for low-T deposition, the weak decrease of the Au AES intensity observed by increasing the temperature is well understood: the thermal energy given to Ag atoms located at the top of the 3D Ag islands is sufficient to cross the Ehrlich-Schwöbel barrier, giving rise to a smoothing of the 3D Ag islands into monoatomic height Ag layers. This is in perfect agreement with the STM picture presented in Figs. 3(a) and 3(b). Second, a strong increase in the Au AES intensity is evidenced above 350 K for 1 ML, and above 470 K in the case of 3 Ag layers. This can be unambiguously attributed to the migration of Au atoms at the surface, leading to the formation of a $Ag_{1-x}Au_x$ surface alloy. This is also corroborated by the work function measurements presented together with AES data in Fig. 4(b). For a coverage of 1 ML of Ag, a strong increase in the work function from $\Phi^s_{Ag}=4.8$ eV (for 1 Ag layers) to $\Phi^s_{Au}=5.34$ eV is evidenced, identical to the value obtained on the free Au(111) surface. One should remark that it is necessary to anneal the 3 ML film at a rather high temperature to obtain the alloy formation, whereas we already observed a (small) intermixing for room-temperature deposition. From our point of view, this is an indication that the moderate diffusion of Au atoms in Ag islands (around 5%) is driven by the substrate reconstruction more than by surface energy consideration. At $T=600$ K, the herringbone reconstruction is restored with a significant disorder, as revealed by STM measurements presented in Fig. 4(d). This disorder is probably introduced by the gradual dilution of Ag atoms extending deeply in the bulk due to the alloy formation.

4. *The Ag growth on* Au(111)*: Conclusions*

Metal-metal heteroepitaxy is known to lead to various surface reconstructions in the case of strong lattice mismatch. We evidence in this experimental work that a rich phenomenology can be observed even in the case of low lattice mismatch. Indeed, in Ag/Au(111) the pre-existing substrate surface reconstruction strongly influences the epitaxial growth of Ag in two different ways: (i) for room-temperature deposition, a short-range ordered reconstruction is observed on Ag islands very close to the herringbone one observed on the Au(111) substrate; (ii) for low-temperature deposition, a singular self-organized growth of Ag islands with a crescent shape, due to a pinning potential extended on the entire hcp domain and not only at the elbow of the substrate reconstruction as previously observed for transition metals.

The experimental measurements presented here allow us to determine with great accuracy two distinct regimes for the Ag films deposited on Au(111): (1) a (relatively) abrupt Ag/Au(111) interface at room temperature where the interdiffusion is negligible (for $T<T_A$) and in which the layer-by-layer growth mode allows a perfect control of the number of monoatomic Ag layers deposited on Au(111); (2) a $Ag_{1-x}Au_x$ alloy (for $T>T_A$) whose composition depends both on the coverage and on the annealing temperature. In the first case, the number of heavy atoms (Au atoms) close to the surface is perfectly controlled by the number of stacked Ag layers. In the second case, we control the enhancement of the heavy atoms concentration at the surface by annealing the deposited Ag layer. The surface state properties are strongly modified and we have investigated the two different interfaces as presented in the following section.

B. Electronic properties

1. *Shockley state energy in the* 300 K *elaborated films*

In this section, we study the Shockley state in the case of the abrupt Ag/Au(111) interface. The Ag layers have been prepared at room temperature and cooled down to 90 K in the STM or in the ARPES setup less than 5 min after the preparation to avoid any time-dependent intermixing effects. We have checked the morphology by STM and measured the

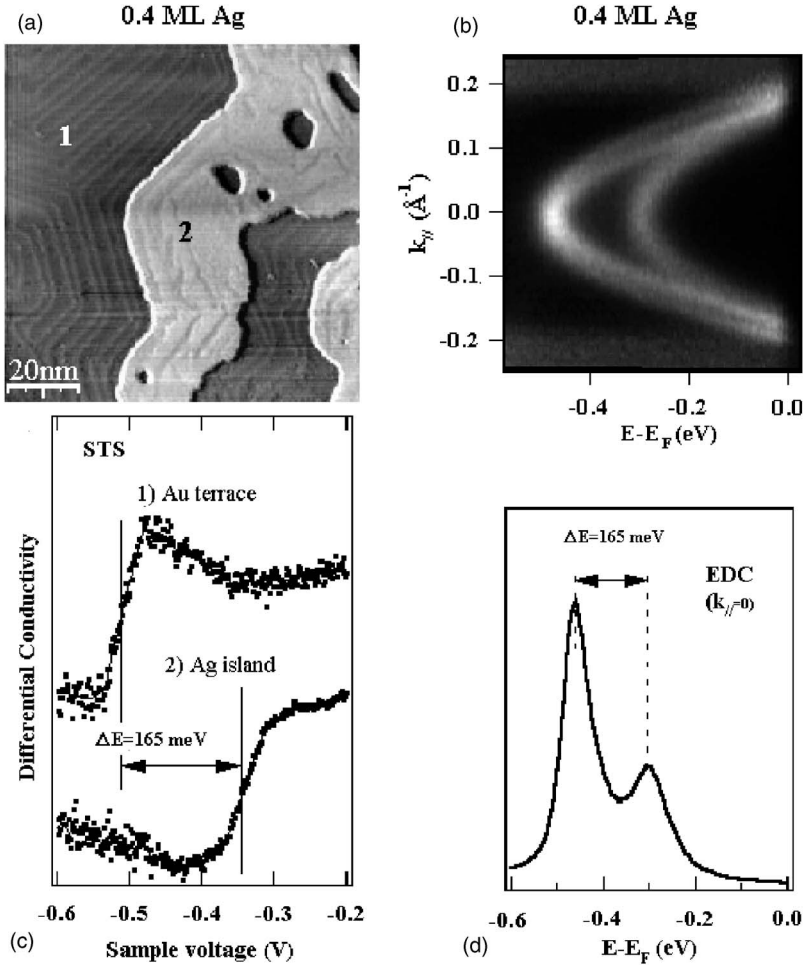

FIG. 5. (a) STM image obtained for 0.4 Ag ML; ARPES intensity map $I(E,k)$ (b) and STS measurements (c) obtained for this coverage; STS curves obtained at 60 K on Au(111) terraces (1) and Ag islands (2) are presented; (d) corresponding EDCs obtained at normal emission in ARPES.

local density of states (LDOS) by recording the differential conductivity dI/dV. ARPES measurements have been performed within 15 min after the introduction in the ARPES setup to avoid contamination at low temperature. Figure 5 summarizes the results we obtained on a 0.4 monolayer Ag film. For this thickness, large Ag islands of monoatomic height and Au(111) substrate area are clearly distinguished [see Fig. 5(a)]. The differential conductivity has been measured on the Au(111) surface and on the Ag islands [Fig. 5(c)]. These two curves present the typical steplike feature signing the 2D k-integrated local density of surface states. As already observed in other noble metal/noble metal interfaces like Ag films deposited on Cu(111),[46] the surface state energy E_0 measured by STS depends on the surface termination: $E_0=-505$ meV for Au-terminated surface and $E_0=-340$ meV for Ag-terminated islands. This behavior has been systematically observed for coverage lower than 1 monolayer, showing that the surface electrons are (partially) confined in Ag islands and Au(111)terraces. The ARPES intensity map $I(E,k)$ measured at $h\nu=21.22$ eV obtained for the same coverage is presented in Fig. 5(b). According to the nearly free electron nature of Shockley states in noble metal, two different surface states exhibiting parabolic dispersions $E(k_{//})=\hbar^2k_{//}^2/2m^*$ are observed with $E_0=-475$ meV and $m^*=0.26\ m_0$ for the deeper one and $E_0=-310$ meV and $m^*=0.33\ m_0$ for the second surface band. Note that the small discrepancy between the binding energies obtained from STS and ARPES measurements (30 meV) is probably due to a small tilt of the normal to the Au(111) surface with respect to the axis analyzer. The deeper band exhibits two k-split parabolas with a splitting of $\Delta k=0.023$ Å^{-1} and can be unambiguously attributed to the Au-terminated Shockley state corresponding to the STS curve number 1. The energy dispersion curves (EDC) taken at normal emission EDC($k=0$), presented in Fig. 5(d) allow us to measure an energy difference of $\Delta E=165$ meV between the two bands. This value is in agreement with STS measurements. As we increase the coverage to 1 monolayer, the peak attributed to Au-terminated surface progressively disappears, whereas the intensity of Ag-island peak increases until the completion of the first layer. Therefore, the energy position of the two surface states remains unchanged and only a redistribution of spectral weight is observed. This leads to the conclusion that the binding energy revealed the surface termination. This behavior has been reported already for Ag films deposited on Cu(111).[55] This has been explained already as resulting from the modification of the surface potential $V(z)$, Ag atoms replacing substrate atoms in the last layer. Indeed, the electronic surface state density probes a modified potential $V(z)$ leading to a change in the surface state binding energy E_0.[46] This is described in detail by the numerical simulations presented in Sec. IV.

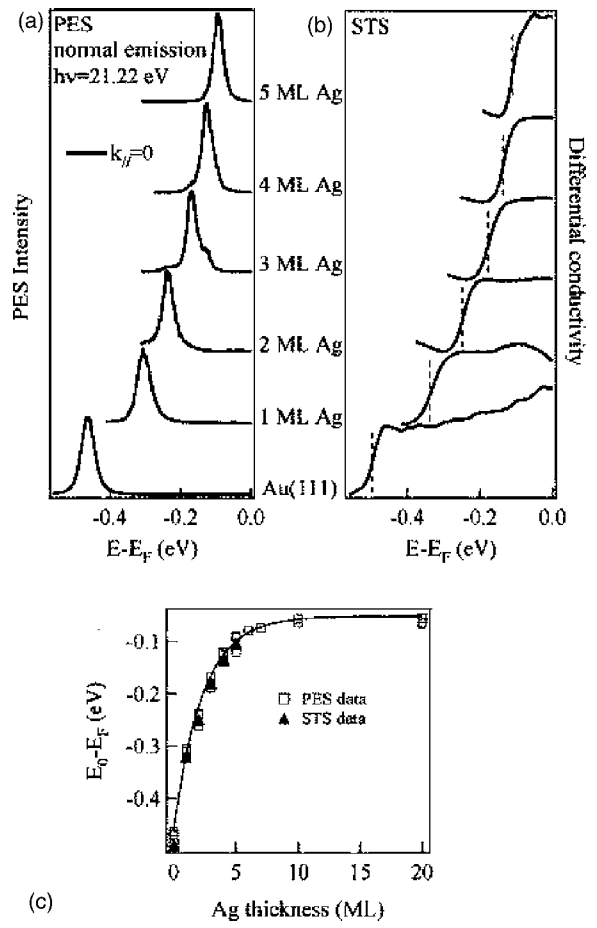

FIG. 6. Normal emission ARPES spectra obtained at 80 K (a) vs STS spectra obtained at 60 K (b); extracted binding energies as function of Ag coverage (c).

The normal emission EDCs and the STS curves are presented for several coverages up to 5 ML in Figs. 6(a) and 6(b). The binding energy of the surface state depends clearly on the number of stacked Ag layers. In addition, for noninteger coverages, two peaks are evidenced in EDCs taken at normal emission, Fig. 6(a). For example, for the case of the deposition of 3 Ag ML presented in Fig. 6(a), the ARPES peak presents a shoulder, indicating that the Ag layer thickness was closer to 3.2 Ag ML (the energy of the additional peak corresponding to the fourth layer). Therefore, the energy of the Shockley state can be used as a probe for the growth mode. The coverage dependence of the surface state energy extracted from STS and ARPES data is presented in Fig. 6(c). The surface state energy evolves from 475 meV for the Au(111) substrate to 60 meV for 20 Ag layers, this value being the typical value measured on Ag(111) single crystals.[56] This behavior has been observed already in ultraviolet photoemission spectroscopy (UPS) measurements on Ag layers deposited on Au(111) (Refs. 57, 58, and 60) and in ARPES for Ag layers deposited on Cu(111).[59,55,46] In our case, the full width at half maximum (FWHM=15 meV) measured by ARPES at $T=90$ K for 20 Ag layers deposited on Au(111) is very close to the best one (FWHM ≈ 9 meV) measured on Ag single crystals at $T=40$ K with the same instrumental resolution.[56] This corroborates the very high quality of the Ag epitaxy on Au(111) substrate. As shown in Fig. 6(c), the binding energy E_0 measured by ARPES and STS as function of the coverage θ can be adjusted by an exponential decay given by

$$E_0(\theta) = E_0^{\mathrm{Ag}} + (E_0^{\mathrm{Au}} - E_0^{\mathrm{Ag}})\exp(-2\beta\theta), \tag{4}$$

with $E_0^{\mathrm{Au}}=-475$ meV, $E_0^{\mathrm{Ag}}=-60$ meV, and $(2\beta)^{-1}=9$ Å. Qualitatively, as far as the coverage increases, the surface state wave function probes less and less the potential of the Au substrate and more and more the potential of the Ag layers. Then, above approximately 10 layers, the bare Ag(111) surface state energy is recovered. This exponential behavior can be understood by a simple first-order perturbation theory as early proposed.[57] Indeed, assuming an exponential decay for the surface state wave function $|\psi(z)|^2 \propto \exp(-2\beta z)$, the variation of the surface state energy as function of the coverage should be given by $E(\theta) \propto \exp(-2\beta\theta)$, $(2\beta)^{-1}$ characterizing the average attenuation length of the surface state in the bulk. Our experimental value $(2\beta)^{-1}_{exp}=3.8$ ML=9 Å is in agreement with the value obtained by Hsieh *et al.*[58] Going beyond first-order theories used to describe Ag/Au(111), Au/Ag(111),[58] and Ag/Cu(111),[55] more quantitative numerical calculations, using the one-dimensional pseudopotential framework proposed by Chulkov *et al.*,[45] have been performed recently in Ag/Cu(111) showing a good agreement with experimental results.[46] New numerical calculations applied to the experimental data presented here are presented in Secs. IV A and IV B.

2. STS on the reconstructed 2nd Ag layer

The long-range herringbone reconstruction observed on the bare Au(111) surface is known to act as a superlattice for surface state electrons.[61] Indeed, the alternation of hcp and fcc domains separated by stacking faults can be approximated by an extended Kronig-Penney model. Therefore, localized states are probed by STS with an electronic density located alternatively in hcp or fcc domains depending on the energy. This was revealed first by the sharp feature obtained by taking the difference between conductance curves measured alternatively on hcp and fcc domains.[61] More recent results allowed us to image the full electronic potential, showing finally that stacking faults constitute the more attractive part of this periodic potential.[62] The back-folded band of the Au(111) surface state due to the $22\times\sqrt{3}$ superstructure has been recently evidenced also by ARPES, but its intensity is only 1/1000 of the main signal.[63] We disregard this effect on ARPES spectra in this paper, especially for Ag ultrathin films due to the disordered nature of the Ag surface reconstruction. In Fig. 7, we focus on STS spectra obtained on the reconstructed second Ag layer, which is also shown to be reconstructed. Numerous STS curves have been recorded with the same tip located above the dark (white points) and bright (black points) domains, these positions being indicated in the STM image of Fig. 7. A systematic deviation can be evidenced by plotting the average of these STS curves taken on each domain as presented in Fig. 7. As already

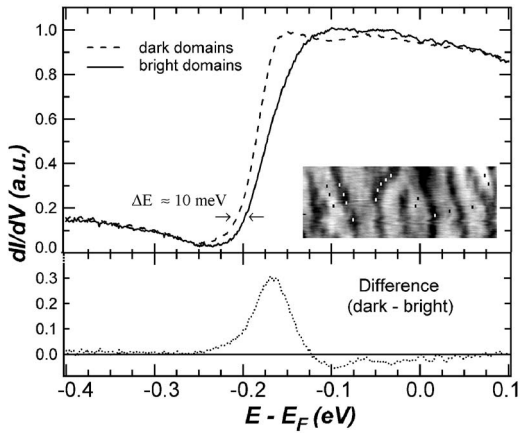

FIG. 7. Top:conductance spectra obtained on bright (dark line) and dark (dashed line) domains; inset: STM image of the reconstructed second Ag layer; bottom: difference between conductance obtained on dark and bright domains.

observed on the free Au(111) surface, the shape of the LDOS differs depending on the type of domains probed. We emphasize this effect by plotting the difference between the average dI/dV curves obtained on each domain (bottom of Fig. 7). This perfectly reproducible effect unambiguously signs a superlattice effect due to the atternation of domains in the superstructure. Therefore, for lower binding energy, the charge density is mainly localized in dark domains. Nevertheless, we would like to mention two major differences compared to what has been observed previously on the Au(111) surface. First, the energy position of the spectroscopic step is systematically different for the two types of domains ($\Delta E \approx 10$ meV). This can be understood as coming from the small intermixing observed at room temperature, which leads to a slightly different concentration in Au atoms in the two kinds of Ag domains (Fig. 2). The 10 meV shift corresponds to few percent of Au inclusions, indicating that we are in the small intermixing limit. Second, the higher spectral weight observed for high binding energies corresponds unambiguously to dark domains. Therefore, since we have attributed these dark areas to fcc stacking (see Sec. III A 1), it appears that the potential modulation induced by this reconstruction is such as (fcc) dark domains are more attractive. Then, it is in clear contradiction to the results obtained on bare Au(111) surface. It is reasonable to think that the Au inclusions can strongly modify the electron potential modulation, this one being more attractive in fcc domains. The STS measurements presented here evidence clearly that the reconstruction observed for Ag thin films deposited on Au(111) induces a superlattice effect as already observed on the bare Au(111) surface, this effect probably being induced by the alternating chemical concentration in Au atoms.

3. Spin-orbit splitting in the 300 K *elaborated films*

In this part, we would like to focus on the evolution of the spin-orbit splitting and the effective mass as function of the coverage. The intensity map $I(E,\theta)$ measured on the Au(111) surface in Ar-I mode ($h\nu = 11.82/11.62$ eV) is presented in Fig. 8. According to the literature,[13,22,27] we observed two parabolic dispersion curves. Indeed, the breakdown of the inversion symmetry at the surface induces a spin-orbit splitting on surface bands. In addition, two sets of two k-split parabola are observed with Ar radiation because of the presence of a double-UV emission line. Due to the conservation law for the parallel component of electron momentum $k_{//} = \sin(\theta)\sqrt{2mE/\hbar^2}$, ARPES measurements taken at low photon energy (Ar-I vs He-I) give a better k-experimental resolution for a given angular resolution. This has been used nicely in the original work of Lashell *et al.*[13] to demonstrate the existence of two Au(111) surface states. As we estimate our angular resolution better than 0.4 deg, we evaluate a k-resolution better than 0.015 Å^{-1} in He-I mode and 0.010 Å^{-1} in Ar-I mode. In the following, we have used both He-I and Ar-I measurements to quantify precisely the surface state parameters in the Ag/Au(111) interface. The momentum dispersion curve (MDC) taken at Fermi energy E_F evidence two peaks for $k_F^- = 0.171$ Å^{-1} and $k_F^+ = 0.194$ Å^{-1}, separated by $\Delta k = 0.023$ Å^{-1} in agreement with previous studies.[13,22] Two features are also clearly visible in the energy dispersion curve (EDC) taken at $k = k_F^-$, evidencing two distinct subbands separated by $\Delta E(k_F) = 110$ meV. Another set of parameters $\Delta k(E_F)$ and $\Delta E(k_F)$ could be extracted from He-I measurements, in perfect agreement with those obtained here with Ar-I. The two dispersion curves, given in Eq. (3), can be expressed in a different way as

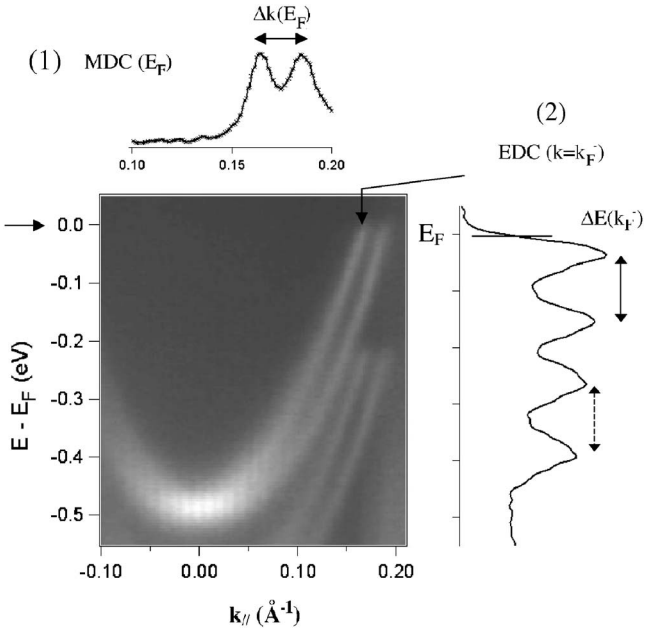

FIG. 8. ARPES intensity map $I(E,k)$ obtained on a Au(111) surface with Ar-I light excitations (the second surface band observed at higher binding energy is due to the presence of a doublet in the light excitation). The momentum dispersion curve measured at E_F is presented in (1); the energy dispersion curve measured at k_F^- is presented in (2).

$$E_{\pm}(k) = \hbar^2(k \pm \Delta k/2)^2/2m^*. \quad (5)$$

Then, the Rashba coupling α_R is deduced both from the

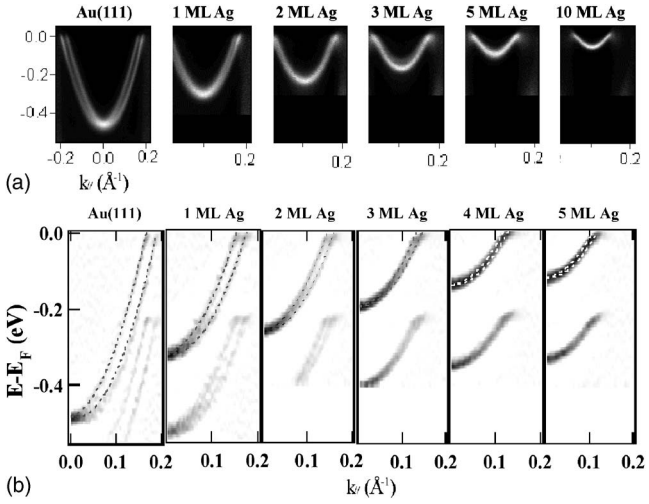

FIG. 9. Coverage dependence of (a) ARPES intensity map obtained with He-I as function; (b) second derivative of Ar-I,II intensity map.

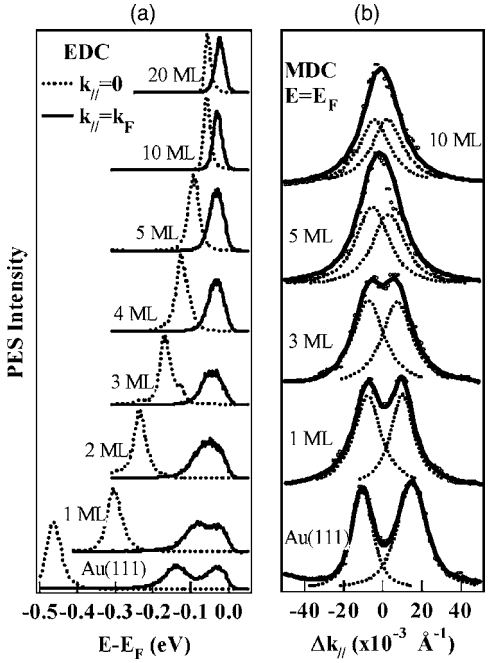

FIG. 10. Coverage dependence of the EDCs at $k=0$ and $k=k_F$ (a) and MDCs at E_F (b) extracted from He-I measurements; experimental data have been fitted by two Lorentzians (dotted lines) to extract the energy and wave vector splitting as explained in Fig. 8.

k-splitting $\Delta k(E_F)$ or from the energy splitting $\Delta E(k_F)$ by using

$$2\alpha_R = \hbar^2 \Delta k_{//}/m^* = \Delta E(k_F^-)/k_F^-. \quad (6)$$

Measuring the position of the bottom of the band $E_0 = 475$ meV and the effective mass $m^* = 0.26 m_0$, and taking into account the energy and wave vector splitting given before, we have obtained a Rashba coupling $2\alpha_R = 0.66 \pm 0.08$ eV Å^{-1} for the Au(111) Shockley state in agreement with previous ARPES results.[13,22] These parameters lead to the correct adjustment of the two experimental parabolic features [as presented in Fig. 9(b)]. Then, starting from the well-defined Au(111) surface state and following the procedure described here, we have measured the Rashba coupling as function of Ag deposition. The He-I intensity map $I(E,k)$ measured for 1,2,3,5, and 10 Ag layers are presented in Fig. 9(a). In addition to the reduction of the binding energy already discussed in the previous section, the effective mass m^* increases continuously whereas the spin-orbit splitting is drastically reduced, the two parabola merging together for thick Ag films. The corresponding second derivative of Ar-I intensity map obtained for 1,2,3,4,5 Ag layers are presented in Fig. 9(b) and evidence that the spin-splitting persists at least up to 3 Ag layers. Detailed EDCs at $k=k_F^-$ and MDCs at $E=E_F$ extracted from He-I measurements are presented in Figs. 10(a) and 10(b). The EDC's at $k=0$ and $k=k_F$ are presented for each coverage investigated. Two well-separated features are evidenced for one Ag monolayer, evidencing the persistence of an energy splitting. Indeed, for higher coverage the two peaks merge into one broad feature, its linewidth being continuously reduced with increasing coverage up to 20 Ag layers. An adjustment of the EDCs with two Lorenztians allowed us to extract the coverage dependence of $\Delta E(k_F)$. In addition, the MDCs taken at the Fermi energy [Fig. 10(b)] evidence the reduction of the k-splitting with increasing the Ag coverage, two features being clearly visible up to 3 monolayers. Again, an adjustment with two Lorentzians allows us to extract the variation of the k-splitting $\Delta k(E_F)$ as function of the Ag coverage. The effective mass m^* increases from 0.265 m_0 for the Au(111) surface state to 0.41 m_0 for the 20 Ag ML surface state. Therefore, by using Eq. (6), we extract the variation of the Rashba coupling upon Ag deposition presented in Fig. 11(a). As previously observed for the coverage dependence of the binding energy, the Rashba parameter follows an exponential decrease given by

$$2\alpha_R(\theta) = 2\alpha_R^{\mathrm{Ag}} + (2\alpha_R^{\mathrm{Au}} - 2\alpha_R^{\mathrm{Ag}})\exp(-2\beta\theta), \quad (7)$$

with $2\alpha_R^{\mathrm{Au}} = 0.66$ eV/Å^{-1}, $2\alpha_R^{\mathrm{Ag}} = 0.11$ eV/Å^{-1} and $(2\beta)^{-1} = 9.5$ Å. The value of 0.11 eV/Å^{-1} extracted for 20 Ag layers is higher than the value of 0.06 eV/Å^{-1} previously reported on a Ag(111) single crystal with comparable ARPES experimental resolution.[63] Nevertheless, they are close within the experimental error bars. The relative variation of E_0, m^*, and α_R are presented in Fig. 11(b), evidencing that both m^* and $2\alpha_R$ scale the variation of the binding energy with Ag coverage. As discussed in the Introduction, in the nearly free electron model, the spin-orbit coupling could depend on the work function. In order to clear up the role of the work function, we attempt to measure its variation induced by Ag deposition. The results are presented in Fig. 11(c). First, the values obtained for the Au(111) surface and for 20 AgML on Au(111) are in good agreement with those given in the literature.[45] Secondly, the work function drops very rapidly to the value measured on free Ag single crystals. Indeed, 60% of the variation is already measured after having completed the first Ag layer and 80% after completion of the second layer. Fig. 11(d) presents a comparison between

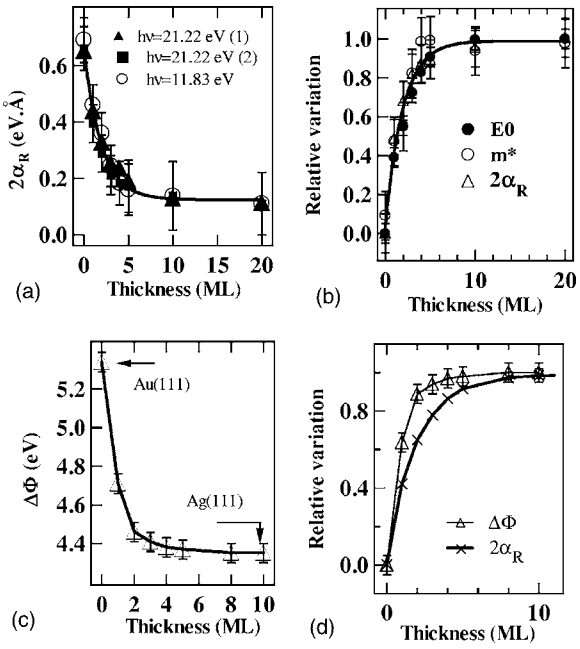

FIG. 11. (a) Rashba coupling obtained in He-I mode from the energy splitting at k_F (black triangles), from the k splitting at E_F (black squares), and from the k splitting at E_F in Ar-I mode (white circles); (b) relative plot of E_0, m^*, and $2\alpha_R$ showing the scaling of all surface state parameters; (c) work function as function of Ag coverage; (d) relative plot of the work function and of the Rashba parameter with Ag coverage.

the adjustment of the relative coverage dependence of $2\alpha_R$ and the work function (Table I).

Clearly, the decrease of the work function is too fast to scale the Rashba parameter. Thus, at this time and in the case of the abrupt interface, we would like to conclude that the exponential variation of the Rashba parameter upon Ag deposition, which quantities the surface state spin-orbit splitting, scales the exponential variation of the binding energy rather than the work function. Note that this result does not exclude the essential role of the surface potential gradient. Indeed, the Rashba effect originates in the symmetry breaking of the surface potential gradient. Beyond the NFE model, tight-binding calculations have evidenced that its amplitude is weighted both by the atomic spin-orbit interaction and the strength of the z-potential gradient at the surface.[26] Assuming ${}^{\mathrm{Au}(111)}W_s / {}^{\mathrm{Ag}(111)}W_s = \simeq 1.2$ and a ratio of 4.3 in their respective atomic coupling (470 meV for Au $6p$ bands and 110 meV for Ag $5p$ bands[27]), assuming the Rashba parameter being proportional to both parameters as proposed in Ref. 26, we expect a faster variation of the Rashba parameter, even faster than the measured work function. At the opposite, the exponential variation of the Rashba parameter is slow, reflecting the strong influence of the attenuation length of the surface state in the bulk. This can be qualitatively understood if we assume that the amplitude of the Rashba parameter is simply given by the number of heavy atoms (Au atoms) probed by the surface state wave function. Then, as for the surface state energy, the pertinent parameter we need to consider is the attenuation length of the Shockley wave function. Such a qualitative assumption is quantitatively described by the numerical simulations presented in Sec. IV.

4. Energy and spin-splitting in the Ag-Au *alloy*

Surface-induced electronic states in ordered solids like noble metals have been the subject of numerous experimental and theoretical studies. At the opposite, disordered alloys having a random crystal potential can exhibit intrinsic surface states, but only few articles based on experimental works are available in the literature. As an example, an intrinsic Shockley-type surface state has been found in the random substitutional $Cu_{0.9}Al_{0.1}(111)$ single-crystal alloy.[64,65] More recently, the electronic structure of ordered and disordered Cu_3Au alloy has been studied: a surface state is still well defined but an additional surface resonance appears due to the displacement of the L-gap edge at higher binding energies.[66–68]

Indeed, although the wave vector $\vec{k}$ is not a good quantum number in disordered alloys, coherent potential approximation (CPA) calculations predict that the Bloch spectral function presents well-defined peaks leading to a well-defined band structure.[69,70] Therefore, gaps are clearly identified and the basic criterion of existence of surface bands is fulfilled. As already discussed in Sec. III A 3, the annealing of the Ag-Au interface yields to the formation of a chemically disordered alloy whose composition depends on (i) the number of stacked layers; (ii) the annealing temperature; and (iii) the annealing duration. To our knowledge, the electronic struc-

TABLE I. Shockley state parameters as function of Ag deposition extracted from ARPES measurements.

Θ (ML)	E_0 (meV) (meV)	m^*/m_0	$\Delta E(k_F)$ (meV)	$\Delta k(E_F)$ (Å^{-1})	$2\alpha_R$ (eV Å)$^{-1}$
Au(111)	475±5	0.265±0.008	110±5	0.023±0.003	0.66±0.079
1	304±5	0.329±0.013	60±5	0.019±0.003	0.394±0.073
2	237±5	0.343±0.016	40±10	0.015±0.003	0.288±0.073
3	168±5	0.378±0.022	26±10	0.013±0.003	0.212±0.073
4	125±5	0.404±0.026	20±10	0.013±0.003	0.184±0.077
5	93±5	0.408±0.028	16±7	0.010±0.003	0.171±0.090
10	59±5	0.400±0.032	10±5	0.007±0.003	0.138±0.120
20	58±5	0.406±0.033	8±5	0.006±0.003	0.110±0.100

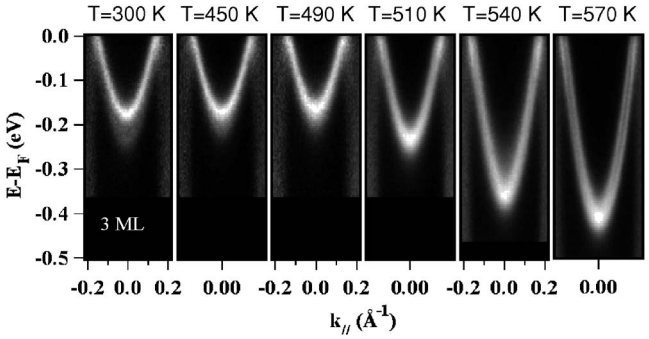

FIG. 12. ARPES He-I intensity map as function of the annealing temperature in the case of 3 Ag ML deposited on Au(111) at room temperature.

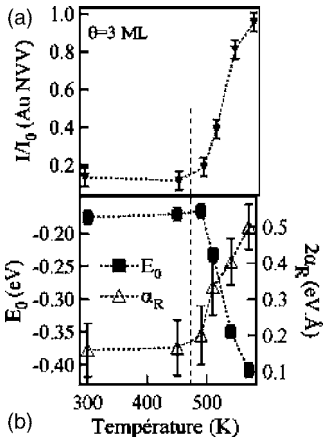

FIG. 13. AES intensity (a), binding energy E_0 and Rashba parameter $2\alpha_R$ (b) as function as the annealing temperature for 3 Ag ML on Au(111).

ture of Au-Ag alloy has been investigated already only in the case of Ag-Au thin layers deposited on Ru(001),[71] but we are not aware of any experimental and theoretical works dedicated to the modification of the Shockley state in such alloys. In addition, the Ag/Au(111) interface provides an opportunity to observe the gradual change of the surface state parameters during the alloy formation (as function of the concentration). The lattice mismatch between bare Au(111) and Ag(111) surfaces is negligible so that Au-Ag alloy shows no significant deviation from the fcc bulk lattice as mentioned previously.[72]

ARPES intensity map $I(E,k)$ measured in He-I on 3 ML Ag deposited on Au(111) as function of the annealing temperature (from 300 to 570 K) are presented in Fig. 12. For 3 Ag ML, the Shockley state is well adjusted by the following parameters: $E_0=168\pm5$ meV, $m^*=0.378$ m_0, $2\alpha_R=0.212\pm0.073$ eV Å^{-1}. For an annealing up to $T=490$ K, no sign of change in surface state parameters is observed, indicating the persistence of a well-defined stacking for Ag layers with negligible intermixing. Above 500 K, AES indicates a Ag-Au intermixing and the binding energy of the surface bands increases continuously to reach a value close to what has been measured on bare Au(111) surface. At the same time, the effective mass decrease and the spin-splitting are restored. At $T=570$ K, we have measured $E_0=440$ meV, $m^*=0.28$ m_0, $2\alpha_R=0.55$ eV Å^{-1}. We have compared the evolution of the Au AES peak intensity [Fig. 13(a)] with the evolution of the surface state parameters, i.e., the binding energy and the Rashba coupling [Fig. 13(b)]. It is clear that, as soon as the AES peak intensity starts to increase, indicating a migration of Au atoms toward the surface, the characteristics of the surface state are strongly modified, reaching those of the Au(111) surface state for temperature higher than 600 K. The linear variation obtained by plotting $2\alpha_R$ and E_0 as function of the AES intensity I/I_0 corroborates this assumption (not presented). It is remarkable that, despite the strong disorder introduced by the formation of the alloy, the Shockley state remains very well defined without any enhancement of its linewidth.

The formation of the Ag-Au alloy with temperature probably leads to a concentration profile for Au atoms, each plane closer to the surface containing less and less Au atoms. A modeling of the alloy concentration profile by a simple one-dimensional diffusion model is presented in Sec. IV C. It is interesting to notice that the mean free path of Auger electron at the kinetic energy of the NVV Au line (69 eV) is of the order of 10 Å and is comparable to the mean free path for photoemitted electron in He-I and to the extension of the surface state wave function in the bulk. Thus, the surface state parameters perfectly scale the AES intensity for each annealing temperature. Therefore, the quantity of Au atoms probed by AES, ARPES, and surface state wave function is approximately the same. As already observed for the abrupt Ag/Au(111) interface, the Rashba coupling scales the Shockley state binding energy as function of the Au enrichment of the surface Ag-Au alloy. The modification of surface state properties in the alloy could be interpreted on different ways. First, in the case of strong lattice mismatch, the position of the surface plane relative to the position of the last atom could lead to a change in the binding energy.[65] This can be excluded in our case due to the too-small lattice mismatch. Second, the bulk band structure should be modified by the alloy formation as mentioned in the case of Cu-Al alloy.[65] In our case, the position of the L-gap for a coverage of 3 ML is rather close to the bare Au(111)surface[33] so that the alloy formation should not affect significantly the L-gap energy position. In addition, it could not explain why the spin-splitting should be affected in the same way. We would like to propose a different scenario which can reconcile both the increase in the surface state binding energy and the increase in the spin-splitting accompanying the formation of the Au enrichment of the surface alloy. In the case of the abrupt interface, described in Sec. IV B, the surface state energy is given by the amplitude of the periodic potential $V(z)$ probed by the surface state wave function, this one being modified by replacing Au by Ag atoms. In the same way, the local on-site potential in the alloy should be modified according to the occupation (or not) by a Au or a Ag atom. An effective potential $V_{eff}(z)$ can be introduced for each subsurface plane. This potential is determined by the respective Au and Ag potential amplitude obtained on the corresponding (111) surface, weighted by the relative concentration of Au and Ag atoms in each subsurface plane. Then, the surface

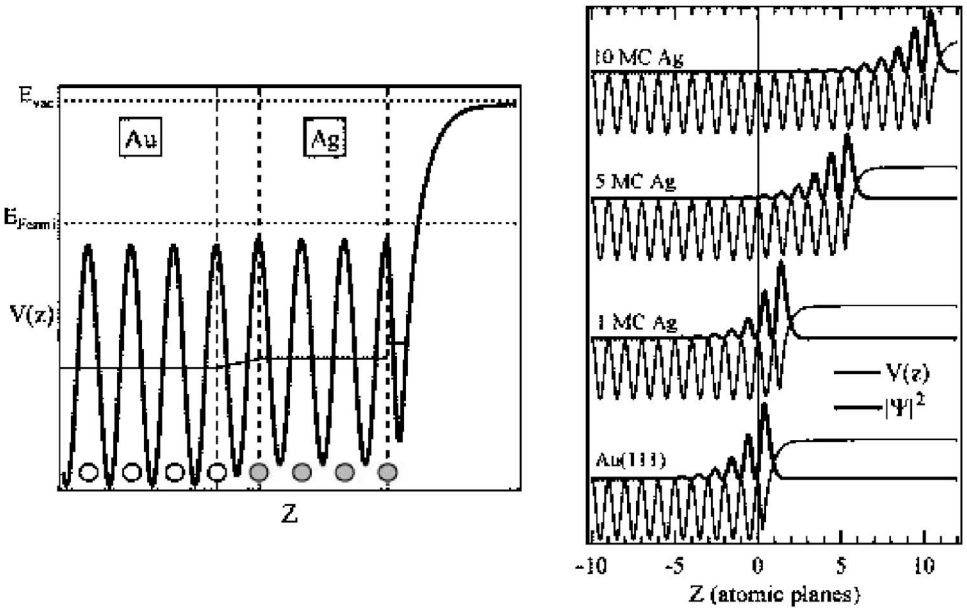

FIG. 14. (a) Modelization of the z potential used to calculate the (pseudo)wave function in the case of 3 Ag layers on Au(111) (parameters are given in the text); (b) coverage dependence of the potential and the electronic density obtained from the calculations.

state energy is determined by the effective potential probed by the surface state wave function. Indeed, as far as the surface is enriched with Au atoms, this effective potential becomes closer to the Au(111) one, in agreement with the surface state energy measured at 570 K. To understand the spin-splitting enhancement with alloy formation, it is natural to invoke the Au enrichment of the surface leading to an increase in concentration of heavy atoms at surface. An effective Rashba parameter can be defined weighted by the number of Au (heavy) atoms probed by the surface state wave function. A more quantitative analysis is presented in the next section devoted to the modeling of the surface state parameters.

IV. MODELING OF THE SHOCKLEY STATE

A. The one-dimensional pseudopotential approach

In order to understand the changes of the surface state parameters upon Ag deposition, the electronic properties of the interface were simulated as a function of Ag thickness. The calculations were based on the one-dimensional pseudopotential introduced by Chulkov *et al.*,[45] and previously used in the case of Ag/Cu(111).[46] The same notations are used in the calculations presented here. A negligible effect of the lateral confinement on the surface state energy due to the large Ag island size justify a one-dimensional approach. A framework based on a pseudopotential with only one Fourier component[45] ($V_G=a_1$) associated with the corresponding reciprocal vector provides a simple approach to obtain the bulk band structure with a gap of magnitude $2\times|V_G|$ at the limit of the Brillouin zone. Therefore, the z-potential, in the direction normal to the surface plane, is approximately sinusoidal inside the Au (Ag) crystal with an average value given by $a_{10}=-10.82$ eV ($a_{10}=-9.27$ eV) referred to the vacuum level and an amplitude $a_1=2.30$ eV (2.15 eV). The shape and height of the vacuum barrier (image state potential) is calculated using the experimentally determined work function $\Phi_s=5.34$ eV (4.29 eV) and adjusting $a_2=3.86$ eV (3.84 eV) and $\beta=4.58$ (4.48). The (pseudo) wave functions and binding energies of the surface state have been calculated using the Numerov algorithm.[73] Using the following two sets of parameters for Au(111) and Ag(111), we have calculated separately the surface state energies of Au(111) and Ag(111) finding $E_0=-485$ meV (-65 meV), respectively, in agreement with ARPES measurements. Then, the potential corresponding to Ag layers deposited on Au(111) is simulated as presented in Fig. 14(a) for the case of 4 ML Ag films prepared at $T=300$ K. The potential can be decomposed into three parts: the Au substrate potential used for pure Au, the interface region, where the potential varies linearly from pure Au to pure Ag (in a first approximation), and the Ag layer, with the potential of pure Ag. All the parameters initially used to simulate separately the Ag(111) and Au(111) surface states are kept constant except a small adjustment of the Au-Ag distance at the interface (less than 0.2 Å).

The calculated electron densities corresponding to several Ag thicknesses are presented in Fig. 14(b). The charge density of the surface state shows an exponential decay in the crystal, as it is expected for a Shockley state, with the main part of the electronic density being localized in the three topmost layers. This result agrees well with the calculations presented in the literature.[60] As the Ag thickness increases, the potential probed by the surface state changes from pure Au to pure Ag, which will induce changes in the wave function and the energy of the surface state [it can be seen in Fig. 14(b) that the decay length of the electronic density increases weakly with increasing Ag thickness].

B. Surface state in the 300 K elaborated films

The modification of the Shockley state parameters upon Ag deposition were first studied in the case of the abrupt interface, which corresponds to the 300 K elaborated films. The calculated binding energies are plotted as a function of Ag thicknesses in Fig. 15(a), together with the PES and STS

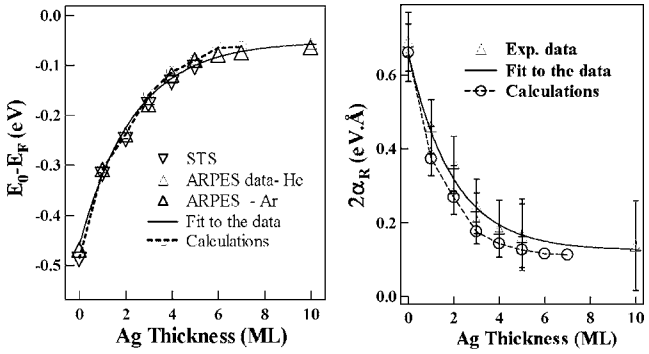

FIG. 15. Comparison between calculated and measured E_0 (a) and $2\alpha_R$ (b); the straight lines are fits of the experimental data; the dotted lines are the calculated ones; triangles are the experimental data.

data for comparison. The overall energy variation is well reproduced within our model. The calculated energy follows the exponential variation experimentally determined, reflecting the decay length of the surface state wave function inside the crystal. By using the calculated wave functions, we have constructed the coverage dependence of the binding energy as an average of the Au and the Ag Shockley state energies, weighted by the relative amounts of the two elements probed by the surface state electron density. The result is presented in Fig. 15(a) and agrees well with experimental data and with simulations. Based on this simple assumption, an effective Rashba parameter was derived for each Ag thickness, as a weighted average of the Au and Ag surface state Rashba parameters, using the calculated electron densities. Indeed, the proportion of Au atoms p^{Au} probed by the surface state wave function is obtained from the decay of the surface state electron density. Then, the Rashba parameter is calculated as follows:

$$\alpha_R(T) = p^{\mathrm{Au}}\alpha_R^{\mathrm{Au}} + (1 - p^{\mathrm{Au}})\alpha_R^{\mathrm{Ag}}, \tag{8}$$

α_R^{Au} and α_R^{Ag} being the Rashba parameter corresponding to bare Au(111) and Ag(111) surface. The results of the model calculations are presented in Fig. 15(b), as well as the experimental data for comparison. The very simple assumption we made allows us to reproduce the experimental data fairly well. This strongly suggests that the amplitude of the Rashba parameter is mainly related to the amount of "heavy" (Au) atoms located in the vicinity of the surface, probed by the surface state. The coverage dependence of the Rashba parameter obtained here with these very simple assumptions is in good agreement with the band structure calculations already published.[33] Nevertheless, the *ab initio* surface state binding energies cannot reproduce the experimental one correctly due to the difficulty getting the Fermi level in density to DFT calculations. The numerical calculations presented here provide the correct experimental values corroborating the scaling between the binding energy and the spin-orbit splitting of the surface state for Ag ultrathin films deposited on Au(111).

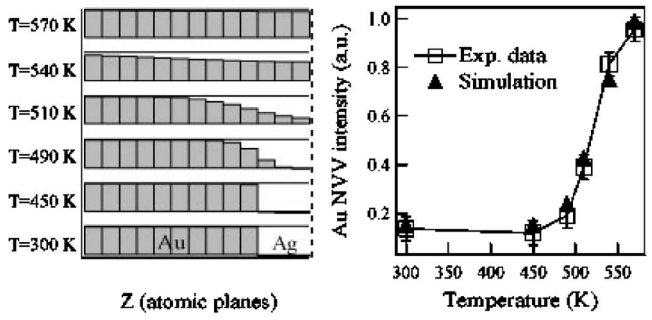

FIG. 16. (a) Concentration profiles obtained from the 1D diffusion model; (b) comparison of the calculated and measured AES data in the case of 3 Ag layers on Au(111).

C. Surface state in the disordered alloy

In a second step, the surface state parameters were calculated in the case of the disordered surface alloy. The Au concentration in each atomic layer was calculated as a function of annealing time and temperature by the use of a one-dimensional diffusion model. The diffusion rate $\nu_0 = 7 \times 10^{16}\ \mathrm{s}^{-1}$ and the activation energy $E_a = 1.83$ eV (Refs. 74 and 75) were adjusted in order to reproduce the experimental Auger Au NVV intensity as a function of temperature. The Auger intensity was calculated assuming an exponential decrease with Ag thickness and a constant electron mean free path $\lambda = 3.54$ ML, estimated from the 300 K measurements. The near-surface concentration profiles calculated for a 3 ML Ag film and the corresponding experimental and calculated Auger Au NVV intensity are presented in Fig. 16(a). One can notice an onset of intermixing from about 490 K, with a fast dilution of the Ag layer in the bulk substrate and an Au enrichment of the surface. After annealing at 570 K the surface is Au-like, with a Ag concentration in the topmost layer less than 5%. This behavior is in good agreement with the ARPES data of Fig. 11, where a Shockley state close to a pure Au(111) surface state is restored.

The concentration profiles were then used to build a pseudopotential $V_{\mathrm{Ag\text{-}Au}}$ for the alloy, as a sum of the Au(V_{Au}) and Ag(V_{Ag}) potentials, weighted by the relative amount of each element in each atomic layer,

$$V_{\mathrm{Ag\text{-}Au}}(z,T) = C_{\mathrm{Au}}(z,T)V_{\mathrm{Au}} + [1 - C_{\mathrm{Au}}(z,T)]V_{\mathrm{Ag}}, \tag{9}$$

$C_{\mathrm{Au}}(z,T)$ being the Au atom concentration at a distance z and for a temperature T, extracted from the diffusion model. The calculated surface state binding energy is plotted as a function of temperature in Fig. 17(a). Once again this very simple model is able to reproduce the experimental data with a satisfying accuracy. The Shockley state energy is related to the amount of Au near the surface: as the surface enriches in Au, the potential near the surface becomes pure Au-like, and the surface state tends to become the pure Au surface state. Based on the same assumptions, an effective Rashba parameter was built in the same way as for the 300 K measurements. Taking into account the decay of the surface state calculated for each temperature (i.e., for each alloy concentration), and the relative amount of Ag and Au atoms in each layer given by the model, one can again deduce the propor-

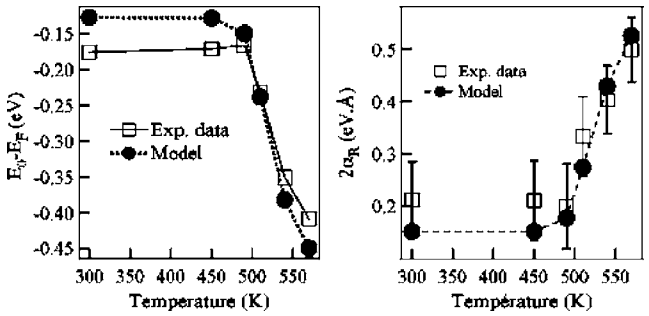

FIG. 17. Comparison between calculated and measured values of the binding energy E_0 (a) and the rashba parameter $2\alpha_R$ (b) in the Ag-Au alloy.

tion of Au atoms $p^{\mathrm{Au}}(T)$ probed by the Shockley wave function which is now T dependent. Then, we calculate the effective Rashba parameter corresponding to an annealing temperature with Eq. (8). The results are shown in Fig. 17(b), and agree surprisingly well with the experimental data for such a simple model. Again, it appears that both the binding energy and the spin-orbit coupling are determined by the number of heavy atoms (Au) probed by the surface state.

V. CONCLUSIONS

Our results strongly suggest that the amplitude of the Rashba (spin-orbit) parameter is mainly determined by the amount of "heavy" atoms probed by the surface state. This has been experimentally evidenced by changing the number of heavy atoms located in the vicinity of the surface by adjusting (i) the number of stacked Ag layers and (ii) by adjusting the concentration of Au atoms in the Ag-Au alloy. This strong dependence of the spin-orbit coupling on the local nature of the elements in the vicinity of the surface shows that the atomic potential is the main factor that determines the amplitude of the Rashba parameter. Indeed, we experimentally demonstrate that the Rashba coupling does not scale the work function in noble metals. In addition, we performed measurements of Shockley state properties in a disordered Ag-Au alloy. Despite this strong chemical disorder, we evidence that the surface state is still well defined for each composition. This has to be considered as the validation of the coherent potential approximation used for band structure calculations in alloys, at least in the case of noble metals whose electronic structures are very similar. The Ag-Au alloy formation gives an opportunity to tune the spin-splitting. This method could be used to increase substantially the energy separation of spin-polarized surface or interface states in order to control spin-polarized transport properties in spintronics devices. Moreover, a comprehensive understanding of the growth of Ag on Au(111) surface has been given. The first, second, and third Ag layers are shown to be reconstructed, this surface reconstruction acting as a superlattice for surface state electrons. Since the mismatch is very weak, the driving force for such reconstruction could be the small Ag-Au intermixing observed at room temperature. Self-organized Ag nanostructures can be obtained at low temperature, Ag atoms being trapped preferentially in hcp domains on flat Au(111) surface. This leads to the possibility to get highly ordered Ag nanostructures on gold vicinal surfaces. An annealing above room temperature allows us to create a Ag-Au alloy with adjustable composition and electronic properties. The systematic study of the structural, chemical, and electronic properties in the same experimental setup by combining STM and/or STS, AES, and ARPES measurements, as presented here, should constitute thekey point to understanding electronic properties in complex systems at surface.

ACKNOWLEDGMENT

We would like to thank S. Pons for his critical reading of this manuscript.

[1] W. Shockley, Phys. Rev. **56**, 317 (1939).
[2] P. O. Gartland and B. J. Slagsvold, Phys. Rev. B **12**, 4047 (1975).
[3] S. D. Kevan, Phys. Rev. Lett. **50**, 526 (1983).
[4] R. Matzdorf, Surf. Sci. Rep. **30**, 153 (1998).
[5] N. Memmel, Surf. Sci. Rep. **32**, 19 (1998).
[6] A. Bendounan, H. Cercellier, B. Kierren, Y. Fagot-Revurat, V. Yu. Yurov, and D. Malterre, Europhys. Lett. **64**, 392 (2003).
[7] R. Otero, A. L. Vasquez de Parga, and R. Miranda, Phys. Rev. B **55**, 10791 (1997).
[8] F. Silly, M. Pivetta, M. Ternes, F. Patthey, J. P. Pelz, and W. D. Schneider, Phys. Rev. Lett. **92**, 016101 (2004).
[9] F. Calleja, V. M. Garcia-Suarez, J. J. Hinarejos, J. Ferrer, A. L. Vasquez de Parga, and R. Miranda, Phys. Rev. B **71**, 125412 (2005).
[10] H. Hövel, B. Grimm, and B. Reihl, Surf. Sci. **447**, 43 (2001).
[11] J. Repp, G. Meyer, and K.-H. Rieder, Phys. Rev. Lett. **92**, 036803 (2004).
[12] A. Mugarza, A. Mascaraque, V. Perez-Dieste, V. Repain, S. Rousset, F.-J. Garcia de Abajo, and J.-E. Ortega, Phys. Rev. Lett. **87**, 107601 (2001).
[13] S. LaShell, B. A. McDougall, and E. Jensen, Phys. Rev. Lett. **77**, 3419 (1996).
[14] C. Tiusan, J. Faure-Vincent, C. Bellouard, M. Hehn, E. Jouguelet, and A. Schuhl, Phys. Rev. Lett. **93**, 106602 (2004).
[15] M. Tinkham, *Group Theory and Quantum Mechanics* (McGraw-Hill, New York, 1964).
[16] R. J. Elliot, Phys. Rev. **96**, 266 (1954); **96**, 280 (1954).
[17] G. Dresselhaus, Phys. Rev. **100**, 580 (1955).
[18] J. R. Chelikowski and M. L. Cohen, Phys. Rev. B **14**, 556 (1976).
[19] E. Rotenberg and S. D. Kevan, Phys. Rev. Lett. **80**, 2905 (1998).
[20] E. Rotenberg, J. W. Chung, and S. D. Kevan, Phys. Rev. Lett. **82**, 4066 (1999).
[21] E. I. Rashba, Sov. Phys. Solid State **2**, 1109 (1960).
[22] G. Nicolay, F. Reinert, S. Hüfner, and P. Blaha, Phys. Rev. B **65**, 033407 (2001).
[23] M. Hochstrasser, J. G. Tobin, E. Rotenberg, and S. D. Kevan,

Phys. Rev. Lett. **89**, 216802 (2002).
[24] M. Muntwiler, M. Hoesch, V. N. Petrov, M. Hengsberger, L. Patthey, M. Shi, M. Falub, T. Greber, and J. Osterwalder, J. Electron Spectrosc. Relat. Phenom. **137-140**, 119 (2004).
[25] J. Henk, A. Ernst, and P. Bruno, Phys. Rev. B **68**, 165416 (2003).
[26] L. Petersen and P. Hedegård, Surf. Sci. **459**, 49 (2000).
[27] F. Reinert, J. Phys.: Condens. Matter **15**, S693 (2003).
[28] H. Cercellier, Y. Fagot-Revurat, B. Kierren, F. Reinert, D. Popovic, and D. Malterre, Phys. Rev. B **70**, 193412 (2004).
[29] H. Cercellier, Ph.D. thesis, Université H. Poincaré, Nancy, France (2004).
[30] M. M. Dovek, C. A. Lang, J. Nogami, and C. F. Quate, Phys. Rev. B **40**, 11973 (1989).
[31] D.-D. Chambliss and R. J. Wilson, J. Vac. Sci. Technol. B **9**, 928 (1991).
[32] H. Cercellier, Y. Fagot-Revurat, B. Kierren, D. Malterre, and F. Reinert, Surf. Sci. **566**, 520 (2004).
[33] D. Popovic, F. Reinert, S. Hufner, V. G. Grigoryan, M. Springborg, H. Cercellier, Y. Fagot-Revurat, B. Kierren, and D. Malterre, Phys. Rev. B **72**, 045419 (2005).
[34] U. Harten, A. M. Lahee, J. P. Toennies, and C. Wöll, Phys. Rev. Lett. **54**, 2619 (1985).
[35] C. Wöll, S. Chiang, R.-J. Wilson, and P.-H. Lippel, Phys. Rev. B **39**, 7988 (1989).
[36] J. V. Barth, H. Brune, G. Ertl, and R. J. Behm, Phys. Rev. B **42**, 9307 (1990).
[37] J. C. Hamilton, R. Stumpf, K. Bromann, M. Giovannini, K. Kern, and H. Brune, Phys. Rev. Lett. **82**, 4488 (1999).
[38] R. Q. Hwang, J.-C. Hamilton, J.-L. Stevens, and S.-M. Foiles, Phys. Rev. Lett. **75**, 4242 (1995).
[39] F. Besenbacher, L. Pleth Nielsen, and P. T. Sprunger, in *Chemical Physics of Solid Surfaces and Heterogeneous Catalysis*, edited by D. A. King and D. P. Woodruff (Elsevier Science Publishers, New York, 1997).
[40] B. Aufray, M. Göthelid, J-M. Gay, C. Mottet, E. Landemark, G. Falkenberg, L. Lottermoser, L. Seehofer, and R. L. Johnson, Microsc. Microanal. Microstruct. **8**, 167 (1997).
[41] I. Meunier, G. Tréglia, J.-M. Gay, B. Aufray, and B. Legrand, Phys. Rev. B **59**, 10910 (1999).
[42] D. D. Chambliss, R. J. Wilson, and S. Chiang, Phys. Rev. Lett. **66**, 1721 (1991).
[43] B. Voigtländer, G. Meyer, and N. M. Amer, Phys. Rev. B **44**, 10354 (1991).
[44] J.-A. Stroscio, D.-T. Pierce, R.-A. Dragoset, and P.-N. Fint, J. Vac. Sci. Technol. A **10**, 1981 (1992).
[45] E. V. Chulkov, V. M. Silkin, and P. M. Echenique, Surf. Sci. **391**, 330 (1997); **437**, L1217 (1999).
[46] A. Bendounan, H. Cercellier, Y. Fagot-Revurat, B. Kierren, V. Yu. Yurov, and D. Malterre, Phys. Rev. B **67**, 165412 (2003).
[47] C. Didiot, S. Vedeneev, Y. Fagot-Revurat, B. Kierren, and D. Malterre, Phys. Rev. B **72**, 233408 (2005).
[48] S. Narasimhan and D. Vanderbilt, Phys. Rev. Lett. **69**, 1564 (1992).
[49] C. E. Bach, M. Giesen, H. Ibach, and T. L. Einstein, Phys. Rev. Lett. **78**, 4225 (1997).
[50] V. Repain, J. M. Berroir, S. Rousset, and J. Lecoeur, Europhys. Lett. **47**, 435 (1999).
[51] Y. Borensztein, T. Lopez-Rios, and G. Vuye, Phys. Rev. B **37**, 6235 (1988).
[52] V. Repain, J. M. Berroir, S. Rousset, and J. Lecoeur, Surf. Sci. **447**, L152 (2000).
[53] J. A. Meyer, I. D. Baikie, E. Kopatzki, and R. J. Behm, Surf. Sci. Lett. **365**, L647 (1996).
[54] C. Didiot, S. Pons, Y. Fagot-Revurat, B. Kierren, and D. Malterre, *Proceedings of the ECOSS 23 Conference*, Surf. Sci. (2006).
[55] A. Bendounan, Y. Fagot-Revurat, B. Kierren, F. Bertran, V. Yu. Yurov, and D. Malterre, Surf. Sci. **496**, L43 (2002).
[56] F. Reinert, G. Nicolay, S. Schmidt, D. Ehm, and S. Hüfner, Phys. Rev. B **63**, 115415 (2001).
[57] T.-C. Hsieh, T. Miller, and T.-C. Chiang, Phys. Rev. Lett. **55**, 2483 (1985).
[58] T.-C. Hsieh and T. C. Chiang, Surf. Sci. **166**, 554 (1986).
[59] A.-P. Shapiro, A. L. Walchs, and T. C. Chiang, Solid State Commun. **58**, 121 (1986).
[60] A. Beckmann, M. Klaua, and K. Meinel, Phys. Rev. B **48**, 1844 (1993).
[61] W. Chen, V. Madhavan, T. Jamneala, and M. F. Crommie, Phys. Rev. Lett. **80**, 1469 (1998).
[62] L. Bürgi, H. Brune, and K. Kern, Phys. Rev. Lett. **89**, 176801 (2002).
[63] F. Reinert and G. Nicolay, Appl. Phys. A: Mater. Sci. Process. **78**, 817 (2004).
[64] W. M. Temmerman, B. L. Gyorffy, and G. M. Stocks, J. Phys. F: Met. Phys. **8**, 2461 (1978).
[65] H. Asonen and M. Pessa, Phys. Rev. Lett. **46**, 1696 (1981).
[66] W. Scott and L. Muldawer, Phys. Rev. B **9**, 1115 (1974).
[67] J. W. Davenport, R. E. Watson, and M. Weinert, Phys. Rev. B **37**, 9985 (1988).
[68] R. Courths, M. Lau, T. Scheunemann, H. Gollisch, and R. Feder, Phys. Rev. B **63**, 195110 (2001).
[69] D. Beaglehole and E. Erlbach, Phys. Rev. B **6**, 1209 (1972).
[70] J. L. Beeby, Phys. Rev. **135**, A130 (1964).
[71] A. Bzowski, M. Kuhn, T. K. Sham, J. A. Rodriquez, and J. Hrbek, Phys. Rev. B **59**, 13379 (1999).
[72] A. I. Frenkel, V. Sh. Machavariani, A. Rubshtein, Y. Rosenberg, A. Voronel, and E. A. Stern, Phys. Rev. B **62**, 9364 (2000).
[73] B. Numerov, Publ. Obs. Central Astrophys. **2**, 188 (1933).
[74] This experimental activation energy is close to the value given in *Introduction to Solid State Physics*, edited by C. Kittel (Wiley, New York, 1986).
[75] P. M. Echenique, J. M. Pitarke, E. V. Chulkov, and A. Rubio, Chem. Phys. **251**, 1 (2000).